RSC Advances

PAPER

View Article Online
View Journal | View Issue

Cite this: *RSC Adv.*, 2022, **12**, 5509

Metal–support interaction induced ZnO overlayer in Cu@ZnO/Al_2O_3 catalysts toward low-temperature water–gas shift reaction†

Zhiyuan Li, *[a] Na Li,[a] Nan Wang,[a] Bing Zhou,[a] Jun Yu,[b] Boyu Song,[b] Pan Yin[b] and Yusen Yang[b]

The water–gas shift reaction (WGSR) plays a pivotal role in many important industrial processes as well as in the elimination of residual CO in feed gas for fuel cells. The development of a high-efficiency low-temperature WGSR (LT-WGSR) catalyst has attracted considerable attention. Herein, we report a ZnO-modified Cu-based nanocatalyst (denoted as Cu@ZnO/Al_2O_3) obtained *via* an *in situ* topological transformation from a Cu_2Zn_1Al-layered double hydroxide (Cu_2Zn_1Al-LDH) precursor at different reduction temperatures. The optimal Cu@ZnO/Al_2O_3-300R catalyst with appropriately abundant Cu@ZnO interface structure shows superior catalytic performance toward the LT-WGSR with a reaction rate of up to 19.47 $\mu mol_{CO}\ g_{cat}^{-1}\ s^{-1}$ at 175 °C, which is ~5 times larger than the commercial Cu/ZnO/Al_2O_3 catalyst. High-resolution transmission electron microscopy (HRTEM) proves that the reduction treatment results in the coverage of Cu nanoparticles by ZnO overlayers induced by a strong metal–support interaction (SMSI). Furthermore, the generation of the coating layers of ZnO structure is conducive to stabilize Cu nanoparticles, accounting for long-term stability under the reaction conditions and excellent start/stop cycle of the Cu@ZnO/Al_2O_3-300R catalyst. This study provides a high-efficiency and low-cost Cu-based catalyst for the LT-WGSR and gives a concrete example to help understand the role of Cu@ZnO interface structure in dominating the catalytic activity and stability toward WGSR.

Received 26th October 2021
Accepted 25th January 2022

DOI: 10.1039/d1ra07896h

rsc.li/rsc-advances

Introduction

The water–gas shift reaction (WGSR) is an industrially important reaction to generate H_2, and is used in numerous relevant chemical industry processes, such as methanol synthesis and steam reforming, coal gasification and ammonia synthesis.[1,2] The WGSR has received increasing attention in the removal of nocuous CO to obtain pure hydrogen for fuel cells.[3–9] This reaction is a reversible exothermic reaction ($CO + H_2O \leftrightarrow CO_2 + H_2$, $\Delta H = -41.2$ kJ mol^{-1}), which is thermodynamically favored at low temperature, while faster reaction rates can be achieved at higher temperatures due to kinetic limitations.[10] Even though this reaction is incompatible in dynamics and thermodynamics, the high CO conversion could be obtained by two-stage system in industry. Typically, in such a system, the Fe_2O_3–Cr_2O_3 catalysts operate at a high temperature range (350–450 °C), and the Cu–ZnO catalysts operate at a low temperature range (190–250 °C).[11] Although the Cu-based catalysts present some advantages in the LT-WGSR, they provide unsatisfactory activity and suffer from sintering during the reaction. Moreover, the exact role of ZnO is not yet clear.

On account of broad applications and significance of the WGSR, numerous studies have been devoted to develop high-efficiency catalytic systems, in which various oxides or carbides supported the metal phase.[4–6,12] The Au-based and Pt-based catalysts have been investigated in the LT-WGSR by virtue of their excellent reactivities.[11–13] For instance, Flytzani-Stephanopoulos *et al.* substantiated that alumina- or silica-supported Pt-based catalysts with a moderate amount of alkali addition displayed significantly enhanced activity toward LT-WGSR.[6,14] Besides, mononuclear gold dispersed on the inert support was further investigated for the low-temperature WGSR.[15] Recently, the α-MoC-supported Pt and Au catalysts, reported by Ma *et al.*, demonstrated superior efficiencies toward the WGSR at a low temperature.[12,16] However, the stability of the noble metal catalysts under realistic conditions is still problematic, and the high price of precious metals limits their practical applications.[17] Copper appears to be a promising active metal, and the Cu-based catalysts have been extensively studied in the WGSR for their advantages, such as abundant resources, low in cost, and excellent catalytic performance.[18–21]

[a]*Stated Grid Integrated Energy Service Group Co., Ltd, Beijing 100052, P. R. China. E-mail: sailorlzy@163.com; Fax: +86-10-63505555; Tel: +86-10-63505060*

[b]*State Key Laboratory of Chemical Resource Engineering, Beijing Advanced Innovation Center for Soft Matter Science and Engineering, Beijing University of Chemical Technology, Beijing 100029, P. R. China*

† Electronic supplementary information (ESI) available: Fig. S1–S7 and Table S1. This material is available free of charge *via* the internet at http://pubs.acs.org. See DOI: 10.1039/d1ra07896h

The synergistic effect of copper–oxide interface was reported by Plata *et al.*, who revealed that optimizing the oxide phase was crucial to improve the performance of the copper/oxide catalyst toward the WGS reaction, which was proved by the experimental and theoretical studies.[22] It was discovered that highly active sites of the WGS reaction were identified at the copper–oxide interface, and the strong interaction between the Cu and oxide supports optimized the catalyst structures as well.[12,23–27] The $Cu/ZnO/Al_2O_3$ catalyst has been employed as an industrial LT-WGSR catalyst since the 1960s;[28,29] however, the catalyst demonstrates low thermal stability and tends to sinter when the temperature is raised above 200 °C due to the low Tamman temperature, thus leading to a decrease in the catalytic activity.[30–33] Therefore, the $Cu/ZnO/Al_2O_3$ catalyst is required to be prepared in a well-controlled way and operated at lower temperatures. The development of robust non-noble Cu-based catalysts with high activities at lower temperatures is still a challenge and evokes enormous interest.

Layered double hydroxides (LDHs) are a class of two-dimensional layered inorganic materials, whose metallic cations are homogeneously dispersed in the brucite-like layers at the atomic level, showing potential applications as catalyst precursors in heterogeneous catalysis.[34–38] Herein, Cu_2Zn_1Al-layered double hydroxide (Cu_2Zn_1Al-LDH) was synthesized by a coprecipitation method, followed by an *in situ* reduction treatment to obtain $Cu@ZnO/Al_2O_3$ catalysts. The optimal $Cu@ZnO/Al_2O_3$-300R catalyst can efficiently catalyze the low-temperature water–gas shift reaction (LT-WGSR) far better than the commercial $Cu/ZnO/Al_2O_3$ catalyst. The Cu@ZnO interface structure with adequately enriched ZnO in the $Cu@ZnO/Al_2O_3$-300R catalyst provided the best catalytic activity and the lowest apparent activation energy toward the WGSR. Furthermore, the formation of ZnO overlayers was beneficial for the stabilization of Cu nanoparticles, which accounted for the long-term stability of the $Cu@ZnO/Al_2O_3$-300R catalyst under reaction condition. A low-cost, high-efficiency Cu-based catalyst with excellent stability for low-temperature WGSR was obtained, which could be used as a promising industrial LT-WGSR catalyst.

Results and discussion

Morphological characterization

The Cu_2Zn_1Al-LDH precursor was synthesized *via* a coprecipitation method. The XRD pattern of the Cu_2Zn_1Al-LDH precursor (Fig. 1A, curve a) showed characteristic diffraction peaks at 2θ of 11.6°, 23.5°, 34.6°, 39.3°, and 46.9°, which belonged to the CuZnAl–CO_3-LDH phase.[29] The corresponding SEM and TEM images (Fig. 1B and S1†) show irregular nanoplatelets with a mean lateral size of 150 ± 30 nm for the Cu_2Zn_1Al-LDH precursor (thickness ~10 nm). The elemental mapping (Fig. S2†) reveals that the Cu, Zn, Al, and O elements are superimposed and distributed uniformly on Cu_2Zn_1Al-LDHs. After *in situ* pretreatment in a H_2 atmosphere at different temperatures, the Cu_2Zn_1Al-LDH precursor underwent a structural transformation to form ZnO phase-modified Cu nanoparticles (denoted as $Cu@ZnO/Al_2O_3$). The original nanoplatelet structure partially collapsed with a change in the chemical composition and a rough surface, which was observed by SEM and TEM (Fig. 1C and S3†). In the XRD patterns of the reduced $Cu@ZnO/Al_2O_3$ samples (Fig. 1A, curves b–d), the two diffraction peaks at 43.3° and 50.4° were ascribed to the Cu phase (PDF#04-0836), while one weak peak at 36.3° can be observed, which is indexed to the ZnO phase (PDF#36-1451). The weak peak in the XRD pattern probably ascribed to the small particle size and low crystallinity of the Cu and ZnO phases, which is consistent with the TEM results (Fig. 3) explained later. Noteworthily, as the reduction temperature is increased from 300 to 400 °C, $Cu@ZnO/Al_2O_3$-300R, $Cu@ZnO/Al_2O_3$-350R and $Cu@ZnO/Al_2O_3$-400R provide a similar particle size of Cu (~7.5 nm), which is calculated based on the Scherrer equation shown in Table 1, suggesting that the pre-reduction temperature imposes a negligible impact on the particle size of Cu probably owing to the strong interaction between the Cu and ZnO phases. Moreover, the element mapping images of these three catalysts (Fig. S4–S6†) showed a good dispersion of Cu, Zn, Al, and O elements.

Catalytic performances toward LT-WGSR

The catalytic performances of the three $Cu@ZnO/Al_2O_3$ catalysts as well as the commercial $Cu/ZnO/Al_2O_3$ catalyst toward the LT-WGSR were tested from 125 °C to 300 °C at a weight hourly space velocity (WHSV) of 15 700 mL g_{cat}^{-1} h^{-1}. Fig. 2A exhibits the CO conversion as a function of reaction temperature. The commercial $Cu/ZnO/Al_2O_3$ catalyst demonstrated a relatively poor activity, whose CO conversion is only 53.2% at 175 °C and attained ~90% at 275 °C. In contrast, the three $Cu@ZnO/Al_2O_3$ catalysts displayed much higher catalytic activities toward the WGSR at a lower temperature. Particularly, the optimized $Cu@ZnO/Al_2O_3$-300R catalyst exhibited the most superior performance among the other $Cu@ZnO/Al_2O_3$ catalysts and provided a CO conversion of up to 97.5% at 175 °C (Fig. 2A). The reaction rate at 175 °C was examined at a low CO conversion (<15%), as illustrated in Fig. 2B and Table 1, giving the following order: $Cu@ZnO/Al_2O_3$-300R > $Cu@ZnO/Al_2O_3$-350R > $Cu@ZnO/Al_2O_3$-400R > commercial $Cu/ZnO/Al_2O_3$. Furthermore, with a further decrease in reduction temperature to 250 °C or 200 °C, the CO conversion and reaction rate decreased (Fig. S7†). The reaction rate of the $Cu@ZnO/Al_2O_3$-300R sample (19.47 μmol_{CO} g_{cat}^{-1} s^{-1}) is ~5 times larger than that of the commercial $Cu/ZnO/Al_2O_3$ (3.58 μmol_{CO} g_{cat}^{-1} s^{-1}) catalyst. Moreover, $Cu@ZnO/Al_2O_3$-300R of this work displayed the highest reaction rate of 19.47 μmol_{CO} g_{cat}^{-1} s^{-1}, which is superior to the previously reported Cu-based catalysts and even some noble-metal catalysts, such as Au-based catalysts (Table S3†). The apparent activation energies (E_a) were calculated on the basis of Arrhenius plots (Fig. 2C and Table 1), and the $Cu@ZnO/Al_2O_3$-300R sample exhibited the lowest E_a (56.5 kJ mol^{-1}), in line with its highest catalytic activity. Correspondingly, the commercial $Cu/ZnO/Al_2O_3$ catalyst, with the lowest reaction rate, presents the highest E_a (76.1 kJ mol^{-1}), as shown in Fig. S8.† The fact indicated that the reaction is inclined to occur on the $Cu@ZnO/Al_2O_3$-300R sample rather than on the commercial $Cu/ZnO/Al_2O_3$ catalyst. In order to meet the requirements of practical application for fuel

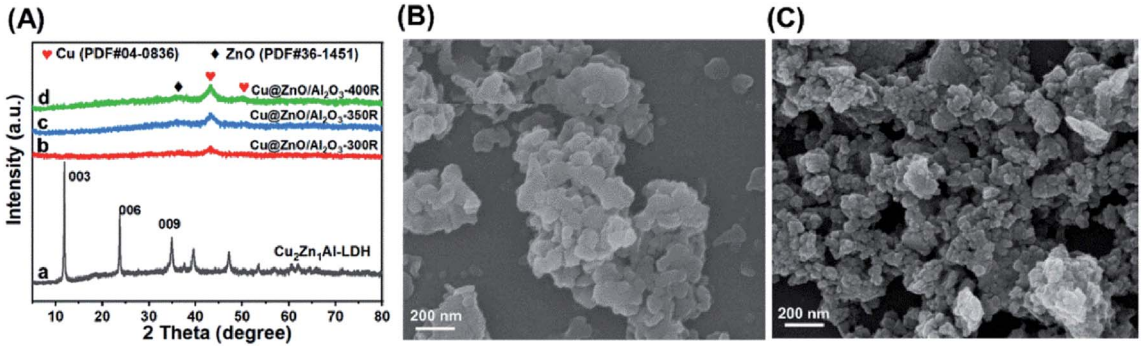

Fig. 1 XRD patterns of (a) Cu_2Zn_1Al-LDH precursor, (b) Cu@ZnO/Al_2O_3-300R, (c) Cu@ZnO/Al_2O_3-350R, and (d) Cu@ZnO/Al_2O_3-400R. (B) SEM image of Cu_2Zn_1Al-LDH precursor. (C) SEM image of reduced Cu@ZnO/Al_2O_3-300R.

cells, the catalysts must go through start/stop cycles of operation. The start-up/shut-down cycle experiment (Fig. 2D) of the Cu@ZnO/Al_2O_3-300R catalyst was carried out to test the recyclability. During each switch, the reaction temperature was increased to 175 °C and maintained for 2 h for catalytic evaluation and then cooled down to room temperature and maintained for another 2 h. After five recycles, a slight drop in CO conversion was observed (from 97.5% to 94.3% at 175 °C) compared with the first cycle (Fig. S9†). Moreover, the TEM image (Fig. S10B†) and element component (Table S1†) of the spent catalyst after five cycles of test showed no apparent change when compared with the fresh catalyst. However, the XRD pattern (Fig. S10A†) shows that the ZnO phase of Cu@ZnO/Al_2O_3-300R after five cycles of test is more pronounced than the fresh one without a negligible size growth of Cu calculated by the Scherrer equation shown in Table S1†. The ZnO phase might excessively deposit on the surface of the active Cu phase, which restricted the contact between the active Cu phase and the reactants, counteracting the reaction. Therefore, the optimized Cu@ZnO/Al_2O_3-300R catalyst shows the highest catalytic efficiency and satisfactory cyclicity.

Structural investigation

TEM and HRTEM were performed to further investigate the particle size of Cu and the structural characteristics of these three Cu@ZnO/Al_2O_3 catalysts (Fig. 3). It is observed that the Cu nanoparticles are uniformly dispersed within the ZnO phase with a very close particle size of ~5.5 nm (Fig. 3A1–C1), which was in accordance with the XRD results (Table 1). As shown in the HRTEM images (Fig. 3A2–C2), the Cu nanoparticles are partially wrapped by the ZnO phase; the clear lattice fringe of 0.245 nm is assigned to the {101} facet of the ZnO phase, while the lattice fringe of 0.206 nm corresponded to the {111} plane of the Cu phase. Furthermore, it is observed that the periphery of Cu nanoparticles is covered by more ZnO overlayers in the Cu@ZnO/Al_2O_3-300R catalyst than that in the Cu@ZnO/Al_2O_3-350R and Cu@ZnO/Al_2O_3-400R catalysts, as shown in the HRTEM images. Alternatively, the Cu@ZnO/Al_2O_3-300R catalyst possessed more abundant Cu@ZnO interface structures than the other two catalysts, which is beneficial to the process of the WGS reaction. This further implied that the Cu@ZnO interface structure in Cu@ZnO/Al_2O_3 is a decisive factor dominating the catalytic efficiency. According to previous studies, the metal phase encapsulated by the support overlayers is deemed as a typical feature of SMSI.[5,32] Thus, the phenomenon with Cu nanoparticles decorated by ZnO overlayers indicated the formation of SMSI in the three Cu@ZnO/Al_2O_3 catalysts. Furthermore, we performed the X-ray excited Auger electron spectroscopy (XAES) measurements to further explore the electronic structure of Cu species. As shown in Fig. S11A,† two peaks are centered at around ~916.2 eV (kinetic energy values) and ~911.0 eV, which belong to the Cu^{2+} and Cu^{+} species, respectively. Notably, the reaction rate as a function of the surface concentration of Cu^{+} species is illustrated in Fig. S11B,† from which a positive correlation is obtained. Therefore, the charge transfer of the Cu–ZnO interface might be the underlying reason to control the catalytic activity, which was in line with the previous reports.[8,13,21–24] However, the direct

Table 1 Physicochemical properties and reaction rates of various Cu@ZnO/Al_2O_3 catalysts

Catalyst	BET surface area ($m^2\ g^{-1}$)	Cu species content[a] (wt%)	Cu crystallite size[b] (nm)	Mean Cu particle size[c] (nm)	Reaction rate[d] ($\mu mol_{CO}\ g_{cat}^{-1}\ s^{-1}$)	E_a (kJ mol^{-1})
Cu@ZnO/Al_2O_3-300R	61.8	27.5	7.6	5.4	19.47	56.5
Cu@ZnO/Al_2O_3-350R	51.8	28.4	7.5	5.5	12.83	58.7
Cu@ZnO/Al_2O_3-400R	54.2	27.8	7.9	5.3	10.31	62.4

[a] Cu species content was determined by using the inductively coupled plasma–atomic emission spectroscopy (ICP–AES). [b] Crystallite size of Cu was determined by XRD using Scherrer equation. [c] Mean particle size of Cu was determined by TEM. [d] Reaction rates were obtained at 175 °C, with a CO conversion below 15%.

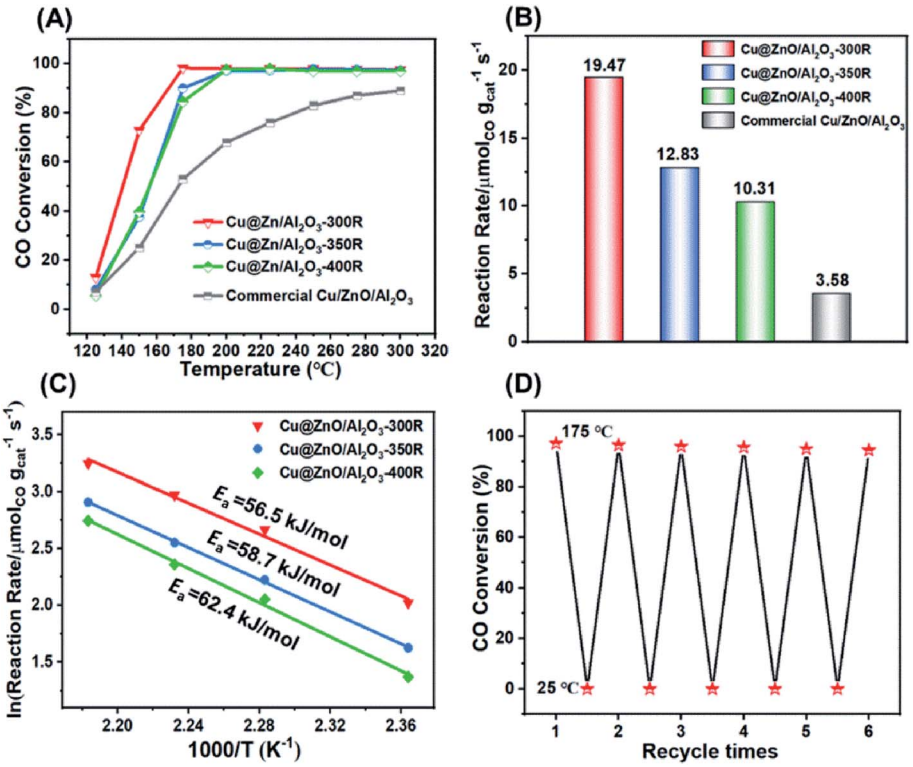

Fig. 2 (A) CO conversion as a function of reaction temperature over the Cu@ZnO/Al_2O_3 catalysts as well as the commercial Cu/ZnO/Al_2O_3 catalyst (WGS reaction conditions: 6% CO, 25% H_2O, 69% Ar; WHSV: 15 700 mL g_{cat}^{-1} h^{-1}). (B) Reaction rates of the Cu@ZnO/Al_2O_3 catalysts and the commercial Cu/ZnO/Al_2O_3 catalyst at 175 °C. (C) Arrhenius plots of the WGS reaction over the three Cu@ZnO/Al_2O_3 samples. (D) CO conversion *vs.* recycle times over the Cu@ZnO/Al_2O_3-300R catalyst (WGS reaction conditions: 6% CO, 25% H_2O, 69% Ar; WHSV: 15 700 mL g_{cat}^{-1} h^{-1}).

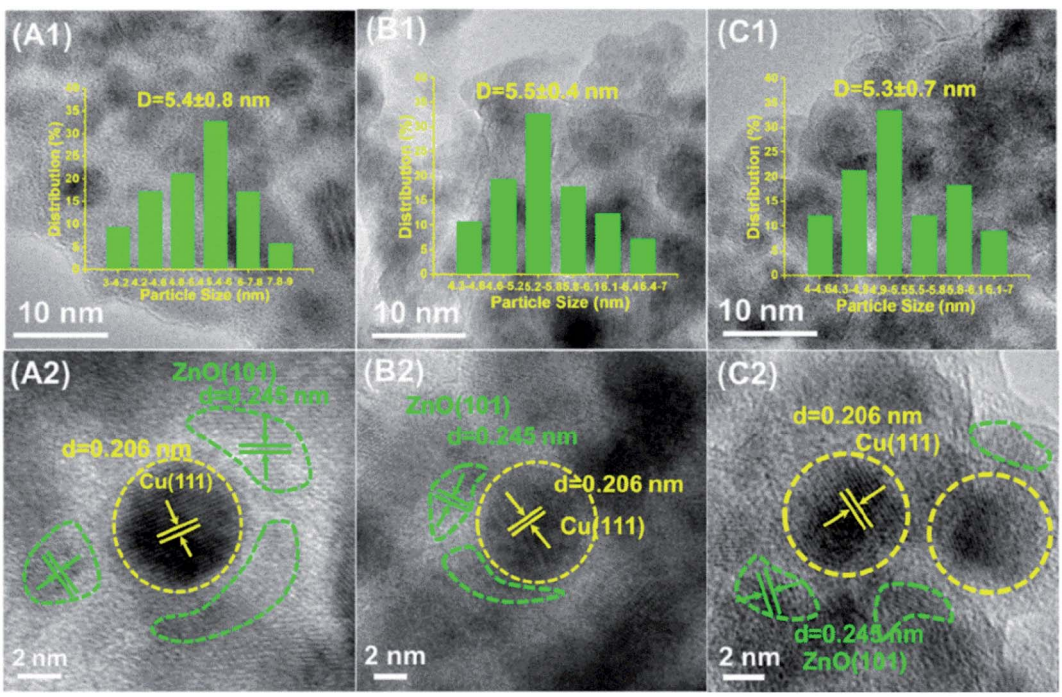

Fig. 3 (A1–C1) TEM images of the three Cu@ZnO/Al_2O_3 samples: (A1) Cu@ZnO/Al_2O_3-300R, (B1) Cu@ZnO/Al_2O_3-350R, and (C1) Cu@ZnO/Al_2O_3-400R. The inset shows the histograms of the size distribution of Cu nanoparticles. (A2–C2) The corresponding HRTEM images of Cu@ZnO interface structure.

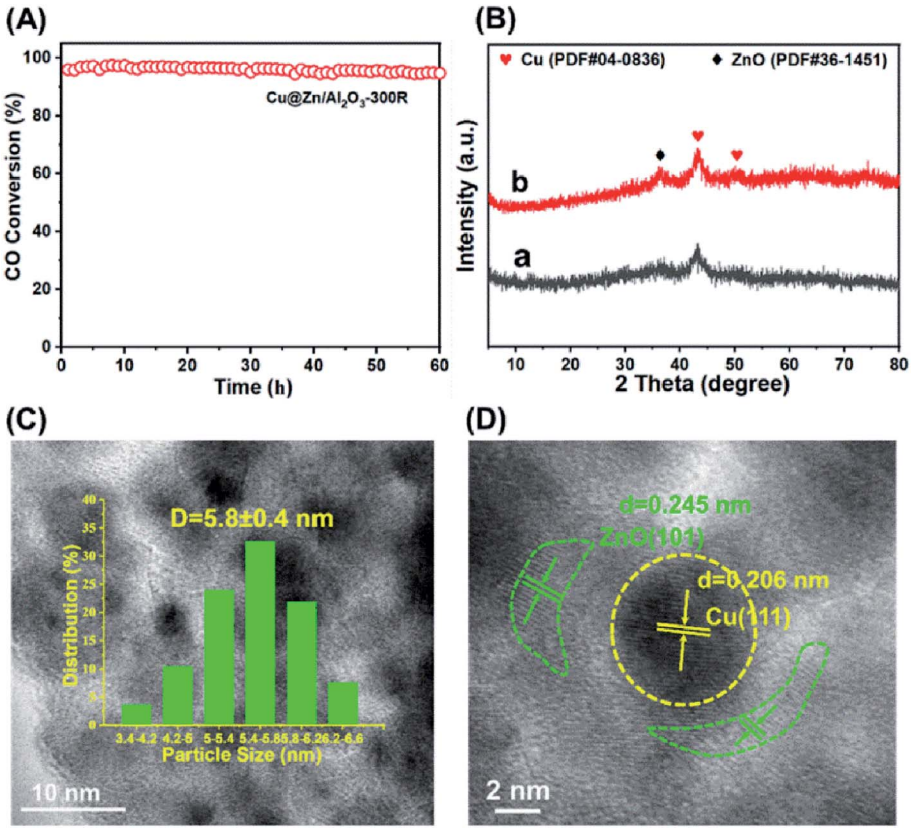

Fig. 4 (A) Plots of CO conversion to CO_2 *vs.* reaction time at 175 °C for the Cu@ZnO/Al_2O_3-300R catalyst. (B) XRD patterns of the Cu@ZnO/Al_2O_3-300R catalyst: (a) the fresh catalyst and (b) the used catalyst after a 60 hour stability test. (C) TEM image of the used Cu@ZnO/Al_2O_3-300R catalyst. (D) HRTEM image of the used Cu@ZnO/Al_2O_3-300R catalyst.

identification of the active interfacial structure should further carry out *in situ*/*operando* characterizations, which will be investigated in our future work.

It is well known that the aggregation of active metals occurred easily for the Cu-based catalysts under the reaction conditions, leading to the deactivation of the catalyst.[31,32] Long-term operation over Cu-based catalysts remained a great challenge. Therefore, we tested the long-term stability of the optimal Cu@ZnO/Al_2O_3-300R catalyst. As shown in Fig. 4A, the Cu@ZnO/Al_2O_3-300R catalyst displays a satisfactory stability with an almost negligible deterioration (from 97.5% to 96%) in catalytic activity toward the WGSR during the 60 hour stability test. However, the Cu particle size of the used Cu@ZnO/Al_2O_3-300R catalyst (Table S2† and Fig. 4C) is slightly larger than that of the fresh catalyst, implying that the Cu phase underwent a slight sintering during the 60 h on stream. Moreover, the XRD peak intensity (Fig. 4B) of the ZnO phase of the used catalyst is stronger than that of the fresh catalyst, suggesting that the ZnO phase is probably further formed under the reaction condition, which is similar to the phenomenon that occurred during the five cycles of test (Fig. S10A†). Little change in the microstructure of the Cu@ZnO interface over the spent Cu@ZnO/Al_2O_3-300R catalyst was observed by HRTEM (Fig. 4D). Due to the Cu@ZnO interface encapsulation structure that the Cu nanoparticles partially modified by ZnO overlayers, the anti-sintering ability of the catalyst is improved under reaction conditions. The above-mentioned results indicated that the Cu@ZnO interface encapsulation structure in Cu@ZnO/Al_2O_3-300R remarkably strengthened the catalytic activity and stability. The formation of the interface encapsulation structure can effectively prevent the sintering of Cu nanoparticles *via* the geometric effect. Therefore, the construction of an active interface structure is of great significance for the preparation of catalysts with high activity and stability.

Conclusion

In summary, the *in situ* reduction process of the Cu_2Zn_1Al-LDH precursor induced the decoration of Cu nanoparticle by the ZnO phase, which resulted in a strong interaction between the Cu and ZnO phases. The impact of the Cu@ZnO interface structure in Cu@ZnO/Al_2O_3 catalysts on the catalytic performance towards WGSR was investigated in detail. The Cu@ZnO/Al_2O_3-300R catalyst exhibited an outstanding catalytic activity towards WGSR due to the abundant Cu@ZnO interface structure, which is directly observed by HRTEM. The reaction rate of Cu@ZnO/Al_2O_3-300R stood at the highest level compared with that of the previously reported Cu-based catalysts. Furthermore, the apparent ZnO coating layers on the Cu nanoparticles helped to anchor the Cu phase, which were responsible for the long-term

stability of the Cu@ZnO/Al_2O_3-300R catalyst under the reaction condition. This study provided a clear and direct evidence that the ZnO overlayers are formed during the pre-reduction process, which is helpful to understand the synergistic effect between Cu and ZnO. Thus, the Cu@ZnO interface structure played a vital role in dominating the catalytic performance towards LT-WGSR.

Experimental section

Raw materials

Analytical grade chemicals, including Na_2CO_3, NaOH, $Cu(NO_3)_2\cdot 3H_2O$, $Zn(NO_3)_2\cdot 6H_2O$ and $Al_2(NO_3)_3\cdot 9H_2O$, were purchased from Sigma Aldrich and used without further treatments. Deionized water was used in the entire experimental process.

Catalyst preparation

The Cu_2Zn_1Al-LDH precursor with $Cu^{2+}/Zn^{2+}/Al^{3+}$ molar ratio of 2 : 1 : 3 was prepared *via* a co-precipitation method. In a typical procedure, $Cu(NO_3)_2\cdot 3H_2O$, $Zn(NO_3)_2\cdot 6H_2O$ and $Al_2(NO_3)_3\cdot 9H_2O$ were fully dissolved in deionized water under ultrasonic treatment to form a homogeneous metal salt solution. Then, the mixed solution and NaOH solution (2 M) were simultaneously added dropwise to a three-necked flask containing Na_2CO_3 aqueous solution (0.1 M) under magnetic stirring. During the process of precipitation, the pH of the mixed solution was strictly controlled at 10 ± 0.2 by a pH meter. The mixture was stirred at room temperature for another 24 h. In order to remove the impurity ions from the precipitation surface, the reaction mixture was centrifuged and washed with deionized water and ethanol repeatedly until the supernatant was neutral. The resulting precipitate was dried in a drying oven at 60 °C overnight to obtain the Cu_2Zn_1Al-LDH precursor. After being ground and sieved, the precursor was directly reduced in the fixed bed before the catalytic evaluation. Correctly, the Cu_2Zn_1Al-LDH precursor was *in situ* reduced in H_2/N_2 stream (2/3, v/v; total flow: 100 mL min^{-1}) at different temperatures for 2 h (heating rate: 5 °C min^{-1}) and then cooled down to room temperature in a high-purity N_2 stream. The as-obtained sample was denoted as Cu@ZnO/Al_2O_3.

Sample characterizations

The content of Cu was determined *via* inductively coupled plasma-atomic emission spectroscopy (ICP-AES). X-ray diffraction (XRD) measurements were carried out on a Rigaku XRD-6000 diffractometer. XRD patterns were recorded by employing a Cu Kα radiation ($\lambda = 0.15418$ nm) at 30 mA and 40 kV over a 2θ angle ranging from 3° to 80° (scanning rate: 5° min^{-1}). Scanning electron microscopy (SEM) images of the samples were obtained on a Zeiss Supra 55 at an accelerating voltage of 20 kV. Transmission electron microscopy (TEM) images were obtained to investigate the particle size and microstructure of catalysts on a JEM-3010 high-resolution transmission electron microscope operating at an accelerating voltage of 200 kV.

Catalytic performance test

A continuous-flow fixed bed with a microquartz tube reactor (8 mm I.D.) was used for the Cu@ZnO/Al_2O_3 catalytic activity evaluation under atmospheric pressure, which was equipped with an online gas chromatograph (GC-2014C Shimadzu). Before the catalytic evaluation, the Cu_2Zn_1Al-LDH precursor dispersed with SiC was pretreated at different temperatures ranging from 300 °C to 400 °C for 2 h in a gas mixture of H_2/N_2 (2/3, v/v) with a total flow of 100 mL min^{-1}. The SiC sand dispersed in catalysts uniformly to make the catalysts touch the feed gas fully. After the cooling down of temperature to 125 °C in a high-purity N_2 stream, the catalysts were exposed to the feed gas (composition: 6%CO/25%H_2O/69%Ar) at a total flow of 110 mL min^{-1}, in which water was introduced into the system by an HPLC pump and mixed with CO/Ar in a vaporizer held at 150 °C. The catalytic performance toward the WGSR was examined from 125 °C to 300 °C, and the weight hourly space velocity (WHSV) was maintained at 15 700 mL g_{cat}^{-1} h^{-1}. Evaluation at each testing temperature was maintained for 2 h in order to make the gas and catalyst in fixed bed reach a stable state and obtain an accurate CO conversion. The composition of gas at the exit of the reactor was analyzed *via* an online gas chromatograph (GC) with a TDX-01 column and a TCD detector, and He was used as the carrier gas. The CO conversion was calculated based on the following formula:

$$X_{CO} = \frac{[CO_2]_{out}}{[CO]_{out} + [CO_2]_{out}} \quad (1)$$

Reaction rate was calculated on the basis of the following equation, and the CO conversion was controlled below 15%:

$$\text{Reaction rate} = \frac{\text{Mol of CO converted}}{\text{mass of catalyst (g)} \times \text{time (s)}} \quad (2)$$

The catalyst was pretreated under the same conditions and exposed to the mixed gas at 175 °C for 60 h, with the data being collected every 0.5 h during the stability test. The start-up/shut-down cycles were performed for five cycles. Concretely, the temperature was raised to 175 °C for 2 h to examine the catalytic activity and then cooled down to atmospheric temperature and maintained for another 2 h.

Conflicts of interest

The authors declare no competing financial interest.

Acknowledgements

This work was supported by the Science and Technology Project of Stated Grid Integrated Energy Service Group Co., LTD

References

1 M. J. L. Ginés, N. Amadeo, M. Laborde and C. R. Apesteguia, Activity and structure-sensitivity of the water–gas shift

reaction over Cu–Zn–Al mixed oxide catalysts, *Appl. Catal., A*, 1995, **131**, 283–296.

2 A. A. Gokhale, J. A. Dumesic and M. Mavrikakis, On the mechanism of low-temperature water gas shift reaction on copper, *J. Am. Chem. Soc.*, 2008, **130**, 1402–1414.

3 H. Yan, C. Yang, W. P. Shao, L. H. Cai, W. W. Wang, Z. Jin and C. J. Jia, Construction of stabilized bulk-nano interfaces for highly promoted inverse CeO_2/Cu catalyst, *Nat. Commun.*, 2019, **10**, 3470.

4 T. Lunkenbein, J. Schumann, M. Behrens, R. Schlogl and M. G. Willinger, Formation of a ZnO overlayer in industrial $Cu/ZnO/Al_2O_3$ catalysts induced by strong metal–support interactions, *Angew. Chem., Int. Ed.*, 2015, **54**, 4544–4548.

5 Z. Zhang, X. Chen, J. Kang, Z. Yu, J. Tian, Z. Gong, A. Jia, R. You, K. Qian, S. He, B. Teng, Y. Cui, Y. Wang, W. Zhang and W. Huang, The active sites of Cu-ZnO catalysts for water gas shift and CO hydrogenation reactions, *Nat. Commun.*, 2021, **12**, 4331.

6 Y. Zhai, D. Pierre, R. Si, W. Deng, P. Ferrin, A. U. Nilekar, G. Peng, J. A. Herron, D. C. Bell, H. Saltsburg, M. Mavrikakis and M. Flytzani-Stephanopoulos, Alkali-stabilized Pt-OH_x species catalyze low-temperature water–gas shift reactions, *Science*, 2010, **329**, 1633–1636.

7 P. Gawade, B. Mirkelamoglu and U. S. Ozkan, The role of support morphology and impregnation medium on the water gas shift activity of ceria-supported copper catalysts, *J. Phys. Chem. C*, 2010, **114**, 18173–18181.

8 S. M. Lee, G. J. Kim, S. H. Lee, I. H. Hwang, S. C. Hong and S. S. Kim, Catalytic performance of $Ce_{0.6}Y_{0.4}O_2$-supported platinum catalyst for low-temperature water–gas shift reaction, *ACS Omega*, 2018, **3**, 3156–3163.

9 H. Yahiro, K. Murawaki, K. Saiki, T. Yamamoto and H. Yamaura, Study on the supported Cu-based catalysts for the low-temperature water–gas shift reaction, *Catal. Today*, 2007, **126**, 436–440.

10 Z. Zhang, S. S. Wang, R. Song, T. Cao, L. Luo, X. Chen, Y. Gao, J. Lu, W. X. Li and W. Huang, The most active Cu facet for low-temperature water gas shift reaction, *Nat. Commun.*, 2017, **8**, 488.

11 R. Tiwari, B. Sarkar, R. Tiwari, C. Pendem, T. Sasaki, S. Saran and R. Bal, Pt nanoparticles with tuneable size supported on nanocrystalline ceria for the low temperature water–gas-shift (WGS) reaction, *J. Mol. Catal. A: Chem.*, 2014, **395**, 117–123.

12 X. Zhang, M. Zhang, Y. Deng, M. Xu, L. Artiglia, W. Wen, R. Gao, B. Chen, S. Yao, X. Zhang, M. Peng, J. Yan, A. Li, Z. Jiang, X. Gao, S. Cao, C. Yang, A. J. Kropf, J. Shi, J. Xie, M. Bi, J. A. van Bokhoven, Y. W. Li, X. Wen, M. Flytzani-Stephanopoulos, C. Shi, W. Zhou and D. Ma, A stable low-temperature H_2-production catalyst by crowding Pt on α-MoC, *Nature*, 2021, **589**, 396–401.

13 J. Dong, Q. Fu, Z. Jiang, B. Mei and X. Bao, Carbide-supported Au catalysts for water–gas shift reactions: a new territory for the strong metal–support interaction effect, *J. Am. Chem. Soc.*, 2018, **140**, 13808–13816.

14 B. Zugic, S. Zhang, D. C. Bell, F. F. Tao and M. Flytzani-Stephanopoulos, Probing the low-temperature water–gas shift activity of alkali-promoted platinum catalysts stabilized on carbon supports, *J. Am. Chem. Soc.*, 2014, **136**, 3238–3245.

15 M. Yang, S. Li, Y. Wang, J. A. Herron, Y. Xu, L. F. Allard, S. Lee, J. Huang, M. Mavrikakis and M. Flytzani-Stephanopoulos, Catalytically active Au-$O(OH)_x$-species stabilized by alkali ions on zeolites and mesoporous oxides, *Science*, 2014, **346**, 1498–1501.

16 S. Yao, X. Zhang, Z. Wu, R. Gao, W. Xu, Y. Ye, L. Lin, X. Wen, P. Liu, B. Chen, E. Crumlin, J. Guo, Z. Zuo, W. Li, J. Xie, L. Lu, C. J. Kiely, L. Gu, C. Shi, J. A. Rodriguez and D. Ma, Atomic-layered Au clusters on α-MoC as catalysts for the low-temperature water–gas shift reaction, *Science*, 2017, **357**, 389.

17 R. Burch, Gold catalysts for pure hydrogen production in the water–gas shift reaction: activity, structure, and reaction mechanism, *Phys. Chem. Chem. Phys.*, 2006, **8**, 5483–5500.

18 M. Konsolakis, The role of copper–ceria interactions in catalysis science: recent theoretical and experimental advances, *Appl. Catal., B*, 2016, **198**, 49–66.

19 J. A. Rodríguez, J. Evans, J. Graciani, J. B. Park, P. Liu, J. Hrbek and J. F. Sanz, High water–gas shift activity in TiO_2(110) supported Cu and Au nanoparticles: role of the oxide and metal particle size, *J. Phys. Chem. C*, 2009, **113**, 7364–7370.

20 L. Yang, A. Karim and J. T. Muckerman, Density functional kinetic Monte Carlo simulation of water–gas shift reaction on Cu/ZnO, *J. Phys. Chem. C*, 2013, **117**, 3414–3425.

21 A. Chen, X. Yu, Y. Zhou, S. Miao, Y. Li, S. Kuld, J. Sehested, J. Liu, T. Aoki, S. Hong, M. F. Camellone, S. Fabris, J. Ning, C. Jin, C. Yang, A. Nefedov, C. Wöll, Y. Wang and W. Shen, Structure of the catalytically active copper–ceria interfacial perimeter, *Nat. Catal.*, 2019, **2**, 334–341.

22 J. J. Plata, J. Graciani, J. Evans, J. A. Rodriguez and J. F. Sanz, Cu Deposited on CeO_x-modified TiO_2(110): synergistic effects at the metal–oxide interface and the mechanism of the WGS reaction, *ACS Catal.*, 2016, **6**, 4608–4615.

23 J. A. Rodriguez, P. Liu, J. Hrbek, J. Evans and M. Perez, Water gas shift reaction on Cu and Au nanoparticles supported on CeO_2(111) and ZnO(000): intrinsic activity and importance of support interactions, *Angew. Chem., Int. Ed.*, 2007, **46**, 1329–1332.

24 J. A. Rodriguez, J. Graciani, J. Evans, J. B. Park, F. Yang, D. Stacchiola, S. D. Senanayake, S. Ma, M. Perez, P. Liu, J. Fdez Sanz and J. Hrbek, Water–gas shift reaction on a highly active inverse CeO_x/Cu(111) catalyst: unique role of ceria nanoparticles, *Angew. Chem., Int. Ed.*, 2009, **48**, 8047–8050.

25 X. Wang, J. A. Rodriguez, J. C. Hanson, D. Gamarra, A. Martínez-Arias and M. Fernández-García, In situ studies of the active sites for the water gas shift reaction over Cu-CeO_2 catalysts: complex interaction between metallic copper and oxygen vacancies of ceria, *J. Phys. Chem. B*, 2006, **110**, 428–434.

26 K. Mudiyanselage, S. D. Senanayake, L. Feria, S. Kundu, A. E. Baber, J. Graciani, A. B. Vidal, S. Agnoli, J. Evans, R. Chang, S. Axnanda, Z. Liu, J. F. Sanz, P. Liu, J. A. Rodriguez and D. J. Stacchiola, Importance of the metal-oxide interface in catalysis: *in situ* studies of the

water–gas shift reaction by ambient-pressure X-ray photoelectron spectroscopy, *Angew. Chem., Int. Ed.*, 2013, **52**, 5101–5105.

27 Y. Bu, C. J. Weststrate, J. W. Niemantsverdriet and H. O. A. Fredriksson, Role of ZnO and CeO_X in Cu-based model catalysts in activation of H_2O and CO_2 dynamics studied by *in situ* ultraviolet–visible and X-ray photoelectron spectroscopy, *ACS Catal.*, 2016, **6**, 7994–8003.

28 N. Koryabkina, A. Phatak, W. Ruettinger, R. Farrauto and E. Ribeiro, Determination of kinetic parameters for the water–gas shift reaction on copper catalysts under realistic conditions for fuel cell applications, *J. Catal.*, 2003, **217**, 223–239.

29 D. Li, S. Xu, Y. Cai, C. Chen, Y. Zhan and L. Jiang, Characterization and catalytic performance of Cu/ZnO/Al_2O_3 water–gas shift catalysts derived from Cu–Zn–Al layered double hydroxides, *Ind. Eng. Chem. Res.*, 2017, **56**, 3175–3183.

30 R. Farrauto, S. Hwang, L. Shore, W. Ruettinger, J. Lampert, T. Giroux, Y. Liu and O. Ilinich, New material needs for hydrocarbon fuel processing: generating hydrogen for the PEM fuel cell, *Annu. Rev. Mater. Res.*, 2003, **33**, 1–27.

31 Y. Dai, P. Lu, Z. Cao, C. T. Campbell and Y. Xia, The physical chemistry and materials science behind sinter-resistant catalysts, *Chem. Soc. Rev.*, 2018, **47**, 4314–4331.

32 L. Wang, L. Wang, X. Meng and F. S. Xiao, New strategies for the preparation of sinter-resistant metal-nanoparticle-based catalysts, *Adv. Mater.*, 2019, **31**, 1901905.

33 A. B. Mhadeshwar and D. G. Vlachos, Is the water–gas shift reaction on Pt simple? Computer-aided microkinetic model reduction, lumped rate expression, and rate-determining step, *Catal. Today*, 2005, **105**, 162–172.

34 G. Fan, F. Li, D. G. Evans and X. Duan, Catalytic applications of layered double hydroxides: recent advances and perspectives, *Chem. Soc. Rev.*, 2014, **43**, 7040–7066.

35 J. Yu, Y. Yang, L. Chen, Z. Li, W. Liu, E. Xu, Y. Zhang, S. Hong, X. Zhang and M. Wei, NiBi intermetallic compounds catalyst toward selective hydrogenation of unsaturated aldehydes, *Appl. Catal., B*, 2020, **277**, 119273.

36 J. Feng, Y. He, Y. Liu, Y. Du and D. Li, Supported catalysts based on layered double hydroxides for catalytic oxidation and hydrogenation: general functionality and promising application prospects, *Chem. Soc. Rev.*, 2015, **44**, 5291–5319.

37 J. Yu, Y. Yang and M. Wei, Preparation and catalytic performance of supported catalysts derived from layered double hydroxides, *Acta Chim. Sin.*, 2019, **77**, 1129–1139.

38 C. Li, M. Wei, D. G. Evans and X. Duan, Layered double hydroxide-based nanomaterials as highly efficient catalysts and adsorbents, *Small*, 2014, **10**, 4469–4486.